

Renormalization-group flow in lattice QED and four-Fermi coupling

Masahiro Imachi

Department of Physics, Kyushu University, Fukuoka 812, Japan

Hiroshi Yoneyama

Department of Physics, Saga University, Saga 840, Japan

(Received 27 February 1990)

Renormalization-group flow of the U(1) lattice gauge theory with staggered fermions is studied by the Migdal-Kadanoff renormalization-group method. The phase structure is extensively investigated. It is shown that an induced four-Fermi coupling term becomes relevant in the strong-gauge-coupling region while it becomes irrelevant in the weak-gauge-coupling one. The β function, the chiral order parameter, and the anomalous dimension of the fermion mass operator are calculated.

I. INTRODUCTION

QED may have a nontrivial fixed point when the gauge coupling becomes strong.¹ Recent studies have shown that the four-Fermi interaction plays an important role with the dynamics governing the strong-gauge-coupling region. It amounts to producing the large anomalous dimension of the fermion mass operator in the low-energy physics, and as a consequence it may open a new possibility toward the origin of the spontaneous breaking of the electroweak gauge symmetry.²⁻⁷

However, it is not yet clear how the four-Fermi interaction concerns itself with original QED. Such an interaction may be induced effectively in the low-energy region from original QED in a nonperturbative manner. To make it clear if it is true or not, a renormalization-group (RG) study⁸ of the theory regularized on the lattice is suitable to this end.

The Migdal-Kadanoff renormalization-group (MKRG) method^{9,10} is an approximate but suitable tool to get into an essential feature of the lattice gauge models.¹¹⁻¹⁶ Such a method may provide us with important information on the dynamics with strong four-Fermi coupling, and is complementary to Monte Carlo calculations which are currently providing interesting results.¹⁷⁻²¹ One of the authors (M.I.) has recently studied the theory by incorporating the fermion self-energy to the recursion equation, and found that the four-Fermi interaction is in fact induced from the original QED in the strong-gauge-coupling region.²² In this paper we make an extensive study of its RG flow and the phase structure.

The main results are as follows. The bare parameter space is divided into two phases, one being the phase where the four-Fermi coupling is relevant and another where it is irrelevant. Within the former phase, there is a distinction with respect to RG flow between the strong-

and weak-gauge-coupling regions. By making use of the unique trajectory (UT) method,⁸ the β function for the gauge coupling is calculated. The chiral order parameter shows a transition separating the two phases. The anomalous dimension γ_m of the fermion mass operator is also calculated by the UT method in the chiral-symmetry-unbroken phase. It is found that γ_m is large at the critical line and monotonically decreases as one goes off from the critical line; i.e., γ_m decreases monotonically as the gauge coupling and/or the four-Fermi coupling C_0 become weak.

In Sec. II the recursion equations are presented. In Sec. III we study the RG flow and the phase structure. Particular attention is paid to the vicinity of the critical line in Sec. IV. The β function and the chiral order parameter are studied in Sec. IV A, and the anomalous dimension of the operator $\bar{\psi}\psi$ is discussed in Sec. IV B. Summary and discussions are presented in Sec. V. An analytic investigation of the recursion equations in the strong four-Fermi coupling region is made in the Appen-

II. MIGDAL-KADANOFF RENORMALIZATION-GROUP TRANSFORMATION

A. Lattice action

The recursion equations for the MKRG transformation for U(1) lattice gauge theory (LGT) with staggered fermions^{23,24} are presented.²²

In general, RG transformations induce couplings which are not in the original bare theory. It is then convenient to write here the most general form of action in the MKRG framework. The lattice action of the U(1) gauge group with staggered fermions ψ and $\bar{\psi}$ is given by

$$\begin{aligned}
 S = S_g + S_f, \quad S_g = -2 \sum_{\text{plaq}} \sum_{q=1}^{\infty} [1 - \text{Re}\chi_q(\theta)]\beta_q, \\
 S_f = A_0 \sum_{n,\mu} \eta_{\mu}(n) [\epsilon_+ \bar{\psi}(n) U_{\mu}(n) \psi(n+\mu) + \epsilon_- \bar{\psi}(n+\mu) U_{\mu}^{\dagger}(n) \psi(n)] - B_0 \sum_n \bar{\psi}(n) \psi(n) \\
 - C_0 \sum_{n,\mu} \bar{\psi}(n) U_{\mu}(n) \psi(n+\mu) \bar{\psi}(n+\mu) U_{\mu}^{\dagger}(n) \psi(n),
 \end{aligned}
 \tag{2.1}$$

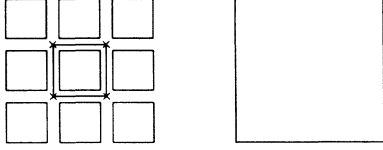


FIG. 1. Gauge plaquette decimation. The vacuum polarization is contained. Crosses denote the fermion decimations. λ is taken to be three.

where χ_q in S_g denotes the q -irreducible character of a plaquette variable; $\chi_q(\theta) = \text{Tr} U_q = e^{iq\theta}$ ($q = \text{integer}$, $0 \leq \theta \leq 2\pi$), and β_q is the corresponding bare inverse gauge coupling. The fermionic action S_f contains three bare parameters, A_0 , B_0 , and C_0 , which represent the hopping parameter, mass, and four-Fermi coupling in turn. Note that the sign convention of C_0 is changed compared with the previous paper,²² and that positive values of C_0 correspond to an attractive force. ϵ_+ and ϵ_- are sign factors ($\epsilon_+ = -1$ and $\epsilon_- = +1$) and $\eta_\mu(n) = (-1)^{n_1 + n_2 + \dots + n_{\mu-1}}$, where n_i is the i th coordinate of the site n . Throughout this paper the following convention for integrating Grassmann variables ψ and $\bar{\psi}$ is employed:

$$\int d\bar{\psi} d\psi \exp(-p\bar{\psi}\psi + \bar{\psi}\xi + \xi\psi) = p \exp\left[\frac{1}{p}\bar{\xi}\xi\right]. \quad (2.2)$$

A RG transformation consists of two procedures: decimation and bond moving, both for the gauge and fermionic degrees of freedom. In each decimation, the gauge degrees of freedom receive fermion loop corrections, while the fermionic ones contain self-energy corrections.

B. Recursion equation for the gauge coupling

The recursion equation for the gauge field¹¹ connecting two scales L and λL is given by

$$F(\lambda L, \theta) = \left[\sum_q \tilde{F}_q(L) \lambda^{2-1} \tilde{Q}_q(L) \chi_q(\theta) \right]^{\lambda^{D-2}}, \quad (2.3)$$

where \tilde{F}_q is a coefficient in the character expansion of the plaquette function $F(L, \theta)$ at scale L ,

$$F(L, \theta) = \sum_q \tilde{F}_q(L) \chi_q(\theta), \quad (2.4)$$

where $F(L, \theta)$ is written in terms of the gauge couplings as

$$F(L, \theta) = F(L, 0) \exp\left[-2 \sum_{q=1}^{\infty} [1 - \text{Re}\chi_q(\theta)] \beta_q(L)\right], \quad (2.5)$$

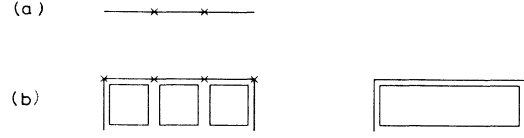


FIG. 2. (a) Link function K . (b) Fermion self-energy correction.

while \tilde{Q}_q is the coefficient in the expansion of $Q(L, \theta)$, which represents the contribution from the innermost plaquette in Fig. 1 receiving the fermion loop correction with N_f flavors (vacuum polarization),

$$Q(L, \theta) = P(\theta)^{N_f} \exp\left[-\sum_q [1 - \text{Re}\chi_q(\theta)] \beta_q\right], \quad (2.6)$$

where

$$P(\theta) = P_0 + P_1 [\chi_1(\theta) + \chi_1^*(\theta)], \quad (2.7)$$

and P_0 and P_1 are given in terms of A , B , and C at scale L as

$$\begin{aligned} P_0 &= 2A^4 + B^4 - 4B^2 A^2 \epsilon_+ \epsilon_- \\ &\quad + 4C(B^2 - \epsilon_+ \epsilon_- A^2) + 2C^2, \\ P_1 &= A^4. \end{aligned} \quad (2.8)$$

The exponent $\lambda^2 - 1$ in (2.3) stands for the decimation of $\lambda^2 - 1$ plaquettes except for the innermost one. [N.B. The contribution of the innermost one is already counted in (2.6).]

A RG transformation is thus completed by bond moving as is represented by the exponent λ^{D-2} in (2.3), which is the contribution from the $D - 2$ directions perpendicular to the plane on which the plaquette in question is sitting.

The left-hand side (LHS) of (2.3) is also represented by the renormalized couplings $\{\beta_q(\lambda L)\}$ at scale λL in the same manner as (2.5):

$$F(\lambda L, \theta) = F(\lambda L, 0) \exp\left[-2 \sum_{q=1}^{\infty} [1 - \text{Re}\chi_q(\theta)] \beta_q(\lambda L)\right]. \quad (2.9)$$

Therefore, by solving (2.3) and (2.9) one obtains the recursion equation for the gauge coupling $\{\beta_q(L)\} \rightarrow \{\beta_q(\lambda L)\}$.

C. Recursion equation for the fermionic couplings²²

As to the fermionic contribution in Fig. 2(a), the link function $K(v)$ is characterized by

$$\begin{aligned} K(v) &= N \exp\{-B(0)\bar{\psi}(0)\psi(0) - B(j+1)\bar{\psi}(j+1)\psi(j+1) + A(0)[\epsilon_+\bar{\psi}(0)U\psi(j+1) + \epsilon_-\bar{\psi}(j+1)U^\dagger\psi(0)] \\ &\quad - C(0)\bar{\psi}(0)U\psi(j+1)\bar{\psi}(j+1)U^\dagger\psi(0)\}, \end{aligned} \quad (2.10)$$

with $j=0$, where N is a normalization constant and v stands for the group element of the link U . The parameters A , B , and C are, by j times decimations [Fig. 2(b)], transformed to

$$\begin{aligned}
N^{(j)} &= N^{(j-1)} N^{(0)} [B^{(j-1)}(j) + B^{(0)}(j)], \quad A^{(j)}(0) = A^{(j-1)}(0) A^{(0)}(j) / [B^{(j-1)}(j) + B^{(0)}(j)], \\
B^{(j)}(0) &= B^{(j-1)}(0) + \Delta B^{(j)}(0), \quad B^{(j)}(j-1) = B^{(0)}(j+1) + \Delta B^{(j)}(j+1), \\
C^{(j)}(0) &= -\Delta B^{(j)}(0) \Delta B^{(j)}(j+1) + A^{(j)2}(0) \epsilon_{\pm}^{(j)} \epsilon_{\pm}^{(j)}, \\
\Delta B^{(j)}(0) &= -[A^{(j-1)2}(0) \epsilon_{\pm}^{(j-1)} \epsilon_{\pm}^{(j-1)} - C^{(j-1)}(0)] / [B^{(j-1)}(j) + B^{(0)}(j)], \\
\Delta B^{(j)}(j+1) &= -[A^{(0)2}(j) \epsilon_{\pm}^{(0)} \epsilon_{\pm}^{(0)} - C^{(0)}(j)] / [B^{(j-1)}(j) + B^{(0)}(j)], \quad \eta^{(j)}(0) = \eta^{(j-1)}(0) \eta^{(0)}(j) \text{ and } \epsilon_{\pm}^{(j)} = \epsilon_{\pm}^{(j-1)} \epsilon_{\pm}^{(0)},
\end{aligned} \tag{2.11}$$

where the notation is that $A^{(j)}(k)$ is a quantity at site k after j decimations have been performed. So the quantities after j decimations are recursively calculated by (2.11) from the ones (2.10) before the decimation.

These parameters then receive self-energy corrections as shown in Fig. 2(b). The convolution of the $\lambda (=j-1)$ plaquettes yields a corrected K_G :

$$\begin{aligned}
K_G &\equiv \int dv K(v) F(v^{-1}w) = \int dv K(v) \sum_q \tilde{F}_q^\lambda(L) \chi_q(v^{-1}w) \\
&= N \tilde{F}_0^\lambda \exp\{-B_G(0) \bar{\psi}(0) \psi(0) - B_G(j) \bar{\psi}(j) \psi(j) + A_G(0) [\epsilon_+ \bar{\psi}(0) U \psi(j) + \epsilon_- \bar{\psi}(j) U^\dagger \psi(0)] \\
&\quad - C_G(0) \bar{\psi}(0) U \psi(j) \bar{\psi}(j) U^\dagger \psi(0)\},
\end{aligned} \tag{2.12}$$

where renormalized parameters are given by

$$\begin{aligned}
A_G(0) &= A^{(j)}(0) \left[\frac{\tilde{F}_1}{\tilde{F}_0} \right]^\lambda, \\
B_G(0) &= B^{(j)}(0), \\
C_G(0) &= C^{(j)}(0) - \left[1 - \left[\frac{\tilde{F}_1}{\tilde{F}_0} \right]^{2\lambda} \right] A^{(j)2}(0) \epsilon_+ \epsilon_-.
\end{aligned} \tag{2.13}$$

A factor \tilde{F}_1/\tilde{F}_0 is analytically represented by the modified Bessel functions as I_1/I_0 for the bare Wilson action. The renormalized parameters obtained in this way are further bond moved in the $D-2$ directions perpendicular to the plaquette in consideration. Namely, each A_G , B_G , and C_G in (2.13) are multiplied by $D-2$. This completes a RG transformation from A, B, C at scale L to the counterparts at scale λL .

Note that the four-Fermi coupling C is not induced by decimations by (2.11); i.e., if one sets $C=0$ on the right-hand side, one sees that C on the left-hand side is identically vanishing. It is self-energy corrections (2.13) that induces C , and its effect is large (small) in the strong-(weak-) gauge-coupling region since $[1 - (\tilde{F}_1/\tilde{F}_0)^{2\lambda}]$ is approximated by $1 - \beta_1^{2\lambda}$ for $\beta_1 \ll 1$ and $O(1/\beta_1)$ for $\beta_1 \gg 1$ (Ref. 22).

It may be convenient to define normalized parameters M and G rather than using A , B , and C . They are defined by

$$M = B/A, \quad G = C/A^2. \tag{2.14}$$

D. Partition function

The partition function Z

$$Z = \int [d\psi d\bar{\psi}] [dU] e^{S_g + S_f} \tag{2.15}$$

is calculated recursively in the Migdal-Kadanoff

renormalization-group approach. The fundamental quantity at each scale is a plaquette and links running along the plaquette. At, say, scale $\lambda'a$ (t times of recursions), by integrating the fermion fields (outermost loop), one is left with only the gauge degrees of freedom to be integrated:

$$Z = \left[\int d\Omega Q(\lambda'a, v) \right]^{D(D-1)/2}, \tag{2.16}$$

where Q is

$$Q(\lambda'a, v) = R(\lambda'a, v)^{N_f} F(\lambda'a, v), \tag{2.17}$$

and $d\Omega$ stands for the group measure over all gauge fields. R in (2.17) is the contribution from the fermionic modes

$$R(a, v) = \int [d\psi d\bar{\psi}] K_{01} K_{12} K_{23} K_{30}, \tag{2.18}$$

where K_{ij} is the link function (2.10) for the link ij , while F is the plaquette contribution.

III. RENORMALIZATION-GROUP FLOW AND PHASE STRUCTURE

We are now ready to calculate RG flow. Throughout this paper the scale factor λ and the number of flavor N_f are taken to be three and unity, respectively. All the calculations in this section are made for a sufficiently small fixed value of $B_0 (=0.05)$. Its extrapolation to $B_0=0$ will be discussed in the following section.

Flow of the renormalization-group transformations by (2.3) and (2.13) runs in the infinite-dimensional parameter space, $(\{\beta_q; q=1 \sim \infty\}, M, G)$. It may then be convenient to project it to various subspaces. In what follows we, in turn, see the one projected to the subspaces of pure gauge (β_1, β_2) , gauge and fermion (β_1, G) , and pure fermion (G, M) .

The flow diagram of gauge couplings is shown for two cases in Fig. 3. One is the case with vacuum polarization

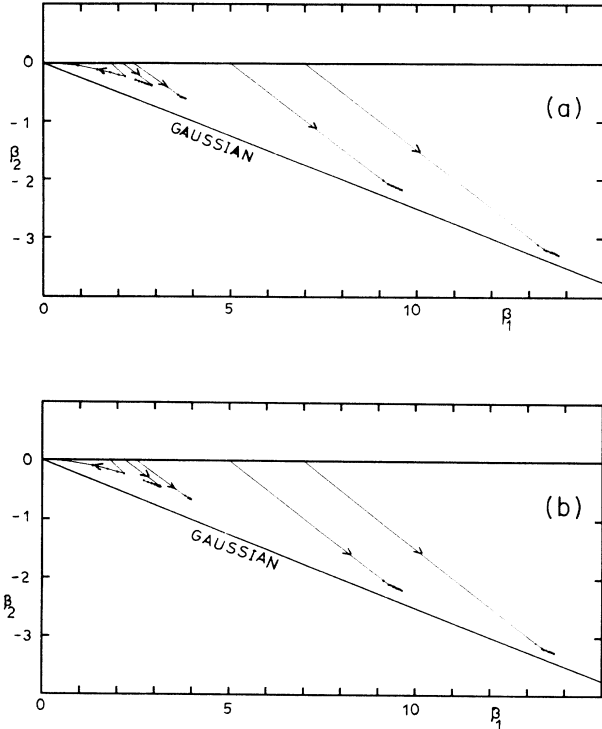


FIG. 3. Flow diagrams of gauge coupling constants projected onto (β_1, β_2) plane. (a) Case with vacuum polarization and without the fermion self-energy correction. (b) Case containing both the effects.

but without the fermion self-energy effect [Fig. 3(a)], and the other is with both effects [Fig. 3(b)]. As seen in Fig. 3(a), trajectories for $\beta_1^0 \leq 2.2$ flow into a fixed point at $\beta_2 = 0$ (strong-coupling phase), and those for $\beta_1^0 \geq 2.3$ flow to larger β_1 along the Gaussian line (weak-coupling phase).

When fermion self-energy is taken into account, the flow shifts a little to stronger coupling; $\beta_1^b = 2.3$ turns to the strong-coupling phase. For $\beta_1^b \geq 2.4$, trajectories flow to a weaker-coupling region. In this case the movement of the trajectories is not so simple due to the roughness of the approximation. For example, starting from $\beta_1^0 = 2.4$, the flow moves to a larger β_1 (namely, weaker coupling) up to $t = 6$, where t is the number of RG transformations. But beyond $t = 6$, couplings move back extremely slowly to smaller β_1 , which we call “switchback.” This behavior does not mean in the strict sense that the corresponding bare theory belongs to the weak-coupling phase. In practice, however, our calculations become poor in precision at large RG steps ($t \approx 6$ in the case of $\beta_1^0 = 2.4$) due mainly to rapid movement of some fermionic parameters. A , in particular, decreases quickly. So it appears reasonable to truncate RG transformations at a reliable step, which coincides with the location where the “switchback” takes place for each bare gauge coupling (e.g., $t = 11-12$ for $\beta_1^0 = 3.0$).

This might partly be due to the limitations of our treatment of vacuum polarization and the self-energy effect.

In our treatment the former may not be taken into account enough, since only the innermost plaquette among λ^2 plaquettes receives the fermionic effect as discussed in (2.6). The result may therefore be too strongly controlled by the fermion self-energy effect. Anyway it appears reasonable to regard in the MK approximation that such “switchback” in the weak-coupling region after many RG steps signals the behavior of the weak-coupling phase.

As to the projection onto the subspace (β_1, G) the RG flow moves as shown in Fig. 4. For each trajectory in the figure, the starting point corresponds to the bare theory with certain (β_1, C_0) . One clearly sees that the two-dimensional subspace (β_1, C_0) is divided into two phases in view of the manner of the movement of the G . For small β_1 and all allowed C_0 values, trajectories move up to the large- G region very quickly. This feature is seen up to the critical point β_c . In the weak-gauge-coupling region beyond β_c , trajectories move up first but eventually go down to small G for small C_0 values, while for large C_0 values the trajectories move up quickly to the large- G region. Namely, inbetween strong and weak four-Fermi coupling regions, a critical line runs (see Fig. 7).

Keeping the above features in mind, let us now see the behavior of the trajectories in the fermionic parameter subspace (M, G) ; for small $\beta_1 (< \beta_c)$.

(1) In the very-strong-coupling region $\beta_1 (< 1.0)$, a range of bare theories in different β_1 and C_0 values moves on to a scaling trajectory as seen in Fig. 5. The functional form of the trajectory reads $G \propto M^2$ for large M and G values.

(2) As β_1 increases beyond 1.0, the flow starts to deviate from such a trajectory, and the slope of the trajectory becomes smaller in the $\log_{10} G - \log_{10} M$ plot.

For large $\beta_1 (> \beta_c)$, the behavior is quite different from

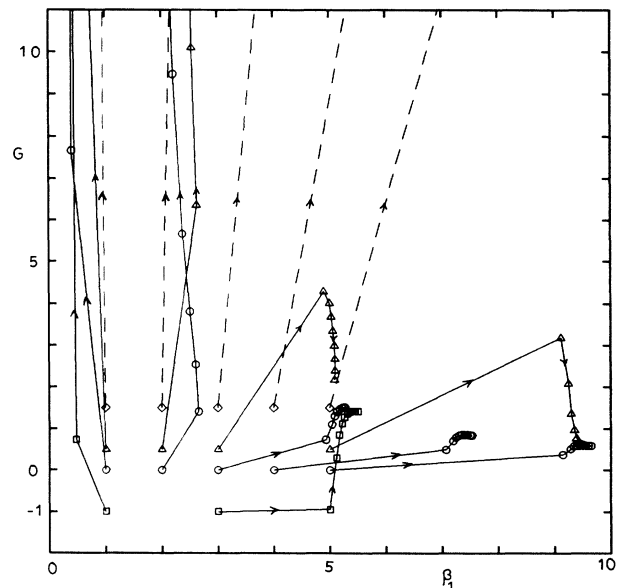


FIG. 4. RG flow projected onto β_1-G plane.

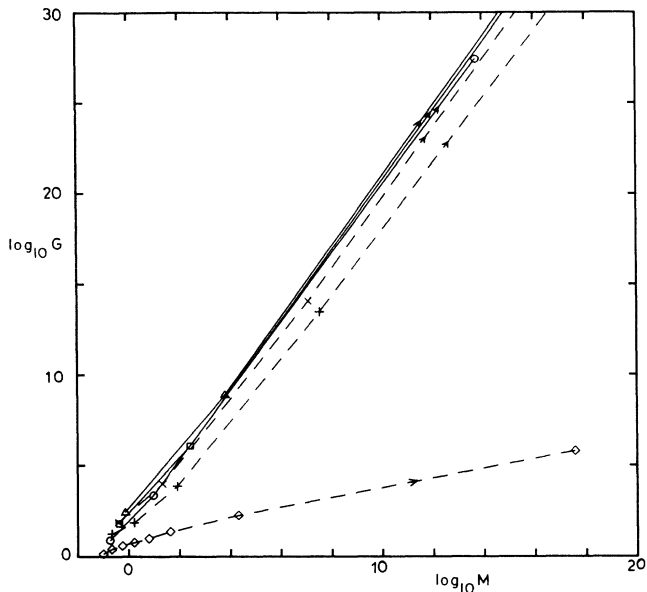


FIG. 5. RG flow projected onto M - G plane. Strong-gauge-coupling case with $\beta_1=1.0$ and $C_0=0.0$ (\circ), 1.0 (\square), and 2.0 (\triangle). Intermediately strong-gauge-coupling case with $\beta_1=2.0$ and $C_0=0.0$ (\diamond), 1.0 ($+$), and 2.0 (\times).

the one for small β_1 .

(1) For large bare C_0 values, the trajectories move up as shown in Fig. 6.

(2) However, for small C_0 values, flows move down and converge to a single trajectory, which moves eventually toward $G=0$.

(3) In between there exists a critical point C_c at which the trajectory becomes flat.

(4) The locations of both the critical C_0 value and the convergent trajectory depend on the chosen β_1 value. As β_1 increases, the value of C_c monotonically increases as seen in Fig. 7. Such a critical line (actually critical surface in the full parameter space) separates the parameter space into chiral-symmetry-unbroken (weak four-Fermi side) and -broken (strong four-Fermi side) phases. This is seen in the following section. A similar critical line is found also in the analysis of the Schwinger-Dyson equation of quenched QED (Ref. 25).

(5) On the other hand, the value of G of the convergent trajectory at sufficiently large M decreases as the bare β_1 increases.

In Fig. 7 the two phases are labeled by I (chiral-symmetry broken) and II (unbroken). Within the chiral-symmetry-broken phase I we found a distinct behavior between strong and weak bare gauge couplings. Trajectories for large bare β_1 values move very slowly toward a larger β_1 value, while those for small β_1 converge rapidly to the fixed point at $\beta_q=0$. This appears to suggest that there is a phase boundary between the two regions. We then distinguish the weaker-gauge-coupling side from the stronger one by naming it the domain III, as indicated in Fig. 7. II and III are then connected to the chiral-symmetry-unbroken and -broken phases, respectively, in the Nambu-Jona-Lasinio model.²⁶

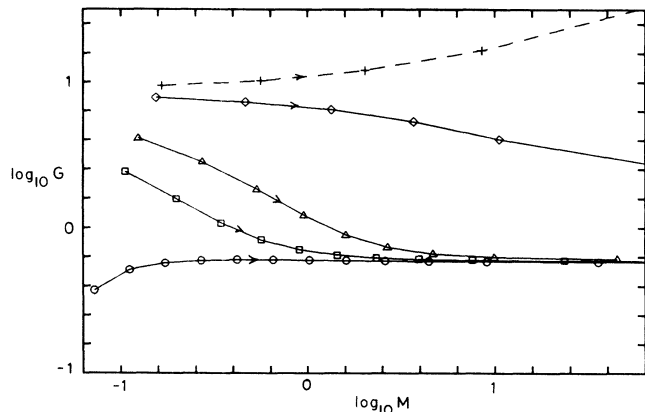


FIG. 6. RG flow projected onto M - G plane. Weak-gauge-coupling case with $\beta_1=5.0$ and $C_0=0.0$ (\circ), 0.4 (\square), 0.6 (\triangle), 0.9 (\diamond), and 1.0 ($+$).

IV. CRITICALITY

A. β function and $\langle -\bar{\psi}\psi \rangle$

In the strong-gauge-coupling region on the Wilson axis, a unique trajectory has been found. Using the unique trajectory method, one calculates the β function.^{8,13,14} Namely, by setting up a renormalized point (called “gate”) on the trajectory at a physical scale ξ_G , and by counting the number of steps of RG transformations t_G to reach the gate from various bare points, one can obtain the β function for the bare coupling β_1 . ξ_G and the lattice constant a are related by $\xi_G = \lambda^{t_G} a$ or $\ln a = -t_G \ln \lambda + \ln \xi_G$. Since ξ_G is independent of a , this equation tells that the β function for β_1 is given by

$$a \frac{\partial \beta}{\partial a} = \frac{-1}{\ln \lambda} \frac{\partial \beta}{\partial t_G} \quad (4.1)$$

or $1/(\partial t_G / \partial \beta^b) \equiv \Phi$ is the Gell-Mann-Low function. In Fig. 8 t_G in the strong-gauge-coupling phase is shown as a function of bare coupling β_1^b , with the gate chosen at

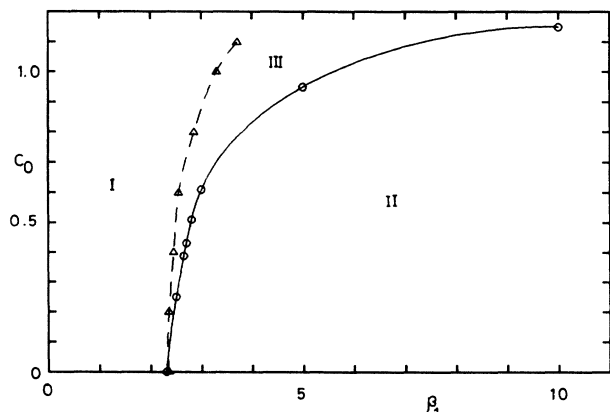
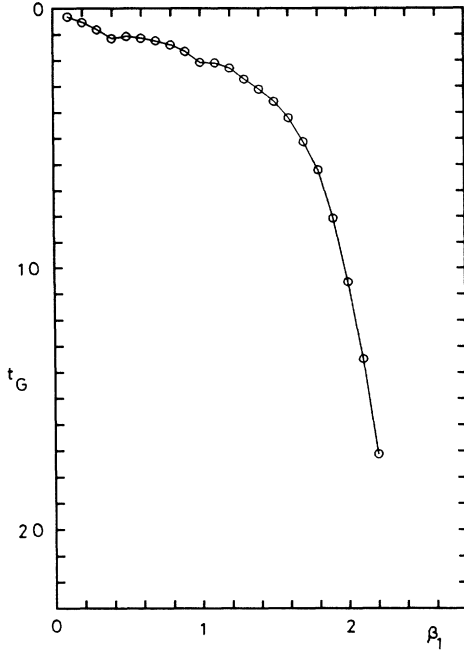


FIG. 7. Phase diagram in β_1 - C_0 plane.

FIG. 8. β_1 - t_G plot for $C_0=0.0$.

$\beta_G = 10^{-3}$. Φ becomes small as $\beta_1 \rightarrow \beta_c$ from below and changes sign at β_c [as can be inferred from Figs. 3(a) and 3(b)].

Chiral order parameter $\langle -\bar{\psi}\psi \rangle$ is calculated from the partition function Z by

$$\langle \bar{\psi}\psi \rangle_{B_0} = \frac{-1}{N_{\text{site}}} \left[\frac{\partial Z}{\partial B_0} / Z \right]_{B_0}, \quad (4.2)$$

and by taking linear extrapolation to $B_0=0$. N_{site} denotes the total site number, λ^{tD} , with t and D being the number of RG iterations and the spacetime dimension ($=4$ in our case), respectively. The result is shown in Fig. 9. We observe that $\langle -\bar{\psi}\psi \rangle$ at strong gauge couplings is much larger than that at weak ones. In the weak-gauge-coupling region, however, $\langle -\bar{\psi}\psi \rangle$ is not exactly zero. Subtracting the value ($\approx 5 \times 10^{-5}$) at large β_1 , therefore, it is fitted by an essential singularity form $\alpha \exp(-\gamma/\sqrt{\beta_c - \beta_1})$. The result is fairly insensitive to the assumed value of β_c . For example, a case for $\beta_c = 2.3$ is shown in the figure.

In Fig. 10 we show the dependence of $\langle -\bar{\psi}\psi \rangle$ on the bare four-Fermi coupling constant C_0 for various bare gauge couplings. In the strong-gauge-coupling region ($\beta_1 = 0.2$ in the figure), all the values are nonzero, which shows the chiral-symmetry-broken phase. In the weak one ($\beta_1 = 5.0$) we observe a transition from the symmetric phase at small C_0 to the broken one at large C_0 ($\gtrsim 1.0$).

B. Anomalous dimension

In this section we discuss the anomalous dimension of $\bar{\psi}\psi$. Figure 11 shows RG flow for various small values of bare mass B_0 in the symmetric phase (or domain II). One sees that all bare theories (for $C_0=0$) with these different

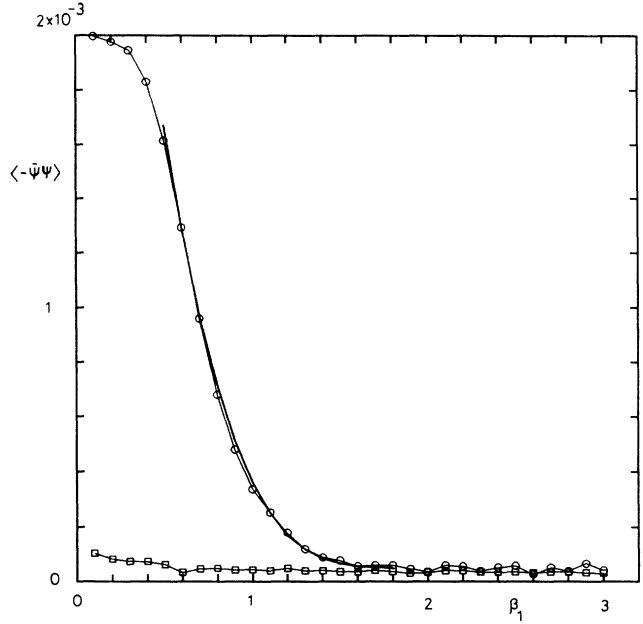


FIG. 9. $\langle -\bar{\psi}\psi \rangle$ vs β_1 . $C_0=0.0$. With fermion self-energy correction (\circ) and without it (\square). The former is fitted by $\alpha \exp(-\gamma/\sqrt{\beta_c - \beta_1})$ with $\beta_c=2.3$, $\alpha=18.14$, and $\gamma=12.50$ (bold line).

different values of B_0 converge to single trajectory. Therefore the unique trajectory method applies in order to get the anomalous dimension of $\bar{\psi}\psi$. That is, one sets up a gate on the trajectory, and then count the number of steps t_G of RG transformations necessary to reach the

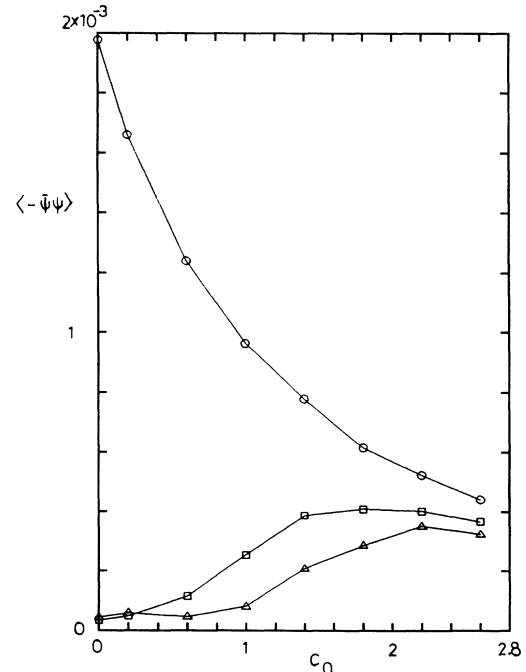


FIG. 10. $\langle -\bar{\psi}\psi \rangle$ vs C_0 for $\beta_1=0.2(\circ)$, $2.0(\square)$, and $5.0(\triangle)$.

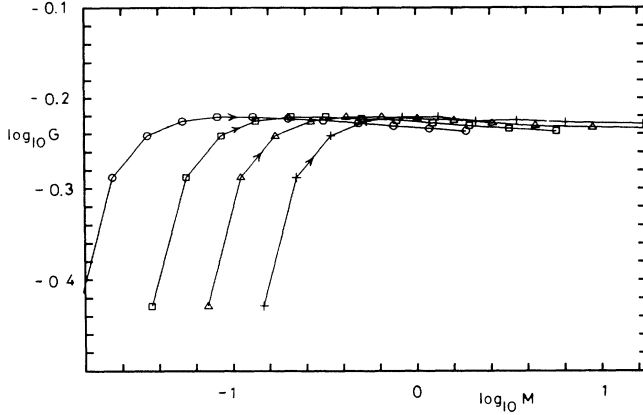


FIG. 11. RG flow projected onto $\log_{10}M$ - $\log_{10}G$ plane for $B_0=0.01$ (\circ), 0.025 (\square), 0.05 (\triangle), and 0.1 ($+$). β_1 and C_0 are chosen to be 5.0 and 0.0 , respectively.

gate from various bare points. The scale at the gate ξ_G and the lattice constant a of a bare point is related by

$$\log_{10}a = -t_G \log_{10}\lambda + \log_{10}\xi_G. \quad (4.3)$$

Figure 12 shows a $\log_{10}B_0 - t_G$ plot for various β_1 values. One sees that for each β_1 , $\log_{10}B_0$ is linear in t_G ,

$$\log_{10}B_0 \approx -c(\beta_1)t_G + d(\beta_1), \quad (4.4)$$

and its slope $c(\beta_1)$ decreases as β_1 increases. The $c(\beta_1)$ is read off to be 0.37 , 0.28 , 0.19 , and 0.14 for $\beta_1=2.5$, 3.0 , 5.0 , and 10.0 in order. This slope is essentially the anom-

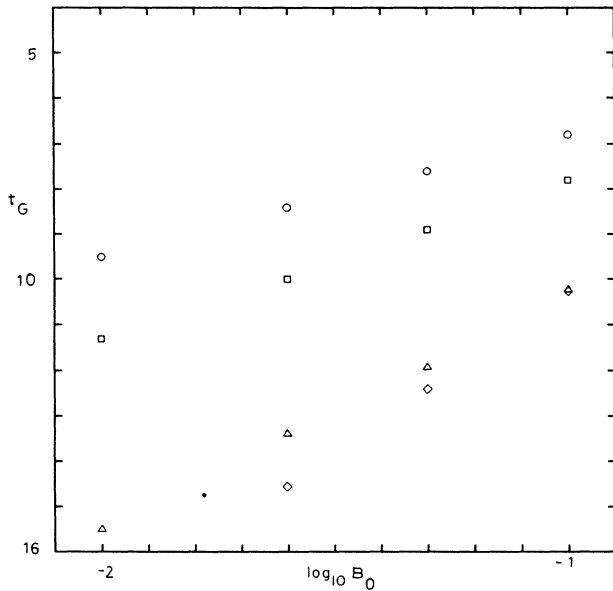


FIG. 12. $\log_{10}B_0$ - t_G plot for $\beta_1=2.5$ (\circ), 3.0 (\square), 5.0 (\triangle), and 10.0 (\diamond). C_0 is chosen to be 0.0 . The gate is chosen in each case at $\log_{10}M_G=1.5$ on the trajectory and the result is insensitive if the gate is set up at $\log_{10}M_G=0.5$ or 1.0 . $\log_{10}M_G$ is taken to be 0.5 for $\beta_1=10.0$ case.

alous dimension of $\bar{\psi}\psi$ as follows.

The anomalous dimension γ_m is defined by

$$\gamma_m = -\frac{\partial \log_{10}m_0(\Lambda)}{\partial \log_{10}\Lambda}, \quad (4.5)$$

where m_0 is a dimensionful bare mass and Λ denotes an ultraviolet cutoff. In the lattice notation, (4.5) reads

$$\gamma_m = \frac{\partial \log_{10}B_0(a)}{\partial \log_{10}a} - 1, \quad (4.6)$$

since $m_0(\Lambda)=B_0(a)/a$ and $\Lambda=1/a$. By using (4.3) and (4.6), γ_m is also represented as

$$\gamma_m = \frac{-1}{\log_{10}\lambda} \frac{\partial \log_{10}B_0}{\partial t_G} - 1. \quad (4.7)$$

For β_1 values in question, (4.4) leads to

$$\gamma_m \approx c(\beta_1)/\log_{10}\lambda - 1. \quad (4.8)$$

For $\lambda=3$, γ_m reads -0.22 , -0.41 , -0.61 , and -0.71 for $\beta_1=2.5$, 3.0 , 5.0 , and 10.0 in turn. This result seems queer, since it is expected that γ_m is positive and becomes vanishing as β_1 goes to infinity, where the theory becomes free. This is due to the quantitative roughness of the approximation. In the free theory, for example, the mass M ought to change to λM by a scale transformation by λ . However, in the MK framework, or rather generally in approximated RG transformations, M does not transform properly¹² but by $\lambda_{\text{eff}}(\neq\lambda)$. Therefore we normalize γ_m in (4.8) so that $\gamma_m=0$ is correctly reproduced in the weak-gauge-coupling limit. Namely, we take λ to be λ_{eff} which is fixed at a large β_1 . We choose $\beta_1=10.0$ (some other choice, say, $\beta_1=15.0$ does not make much difference in the following result). The estimated value of λ_{eff} is 1.39 . This leads to $\gamma_m=1.64$, 1.0 , 0.36 , and 0.0 for $\beta_1=2.5$, 3.0 , 5.0 , and 10.0 (see Fig. 13).

This way of calculations applies to the whole region of the domain II (chiral-symmetry-unbroken phase). Figure 14(a) shows the behavior of γ_m on an axis $C_0=0.6$. It looks almost the same as the one of $C_0=0.0$ case except that the location of the critical point is shifted to the weaker gauge coupling side. Figure 14(b) is, on the other

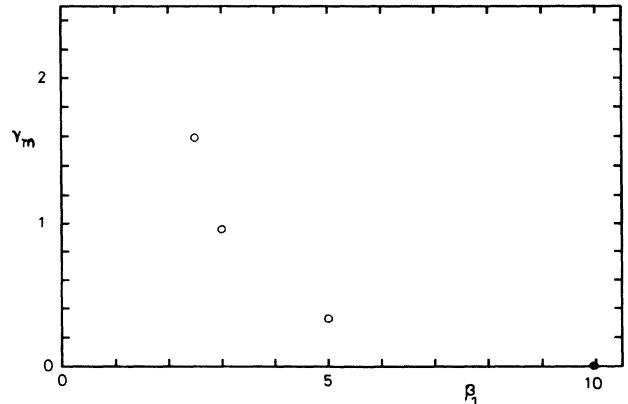


FIG. 13. γ_m vs β_1 for $C_0=0.0$.

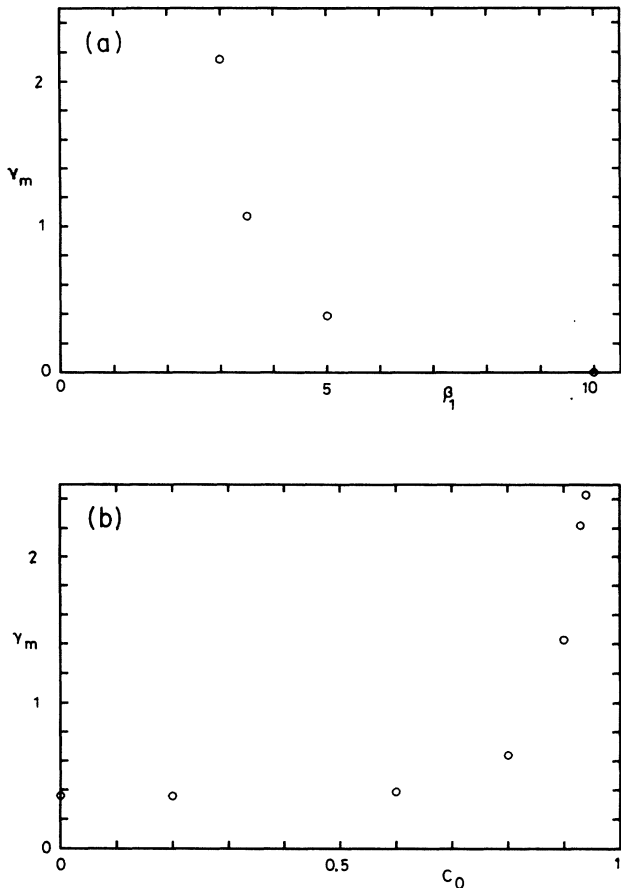


FIG. 14. (a) γ_m vs β_1 for $C_0=0.6$. (b) γ_m vs C_0 for $\beta_1=5.0$.

hand, for an axis $\beta_1=5.0$. The value at $\beta_1=2.5$ in Fig. 13, near the critical point, is fairly large compared to the value 1.0, predicted in the quenched Schwinger-Dyson equation approach.^{3,6} This merely shows to what extent the MKRG is quantitatively precise. The above results are, however, qualitatively good that γ_m is large at the critical point and monotonically decreases as one goes away from the critical point, i.e., as the gauge coupling and/or the four-Fermi coupling becomes weak.

The similar result is also obtained in the calculation of the SU(2) and SU(3) pure gauge theory.^{13,14} There the coefficient of the β function obtained by the UT method depends on the scale factor λ . Qualitatively speaking, however, the MK method predicts correctly the asymptotically free behavior in the weak coupling region as well as the crossover phenomenon in the intermediate coupling region.

V. SUMMARY AND DISCUSSION

We have studied the RG flow of lattice QED in the MKRG approach. Although it is based upon an approximate procedure, it still provides us with interesting results concerning nonperturbative nature of the dynamics of the model. We have seen that the four-Fermi interaction is induced from the original QED and is relevant for the physics in the strong gauge coupling. The RG flow,

the β function (Gell-Mann-Low function), and $\langle -\bar{\psi}\psi \rangle$ show the chiral phase transition. In the broken phase, the four-Fermi coupling increases rapidly, whereas in the symmetric one, it is, although induced, eventually attracted by an infrared stable fixed point at $G=0$. The anomalous dimension γ_m of $\bar{\psi}\psi$ turns out to be large along the critical line in (β_1, G) plane, and monotonically decreases as the gauge and/or the four-Fermi coupling become weak in the chiral-symmetry-unbroken phase.

Some remarks are in order.

A critical line runs in the phase diagram of the fundamental and the adjoint representations of the gauge couplings in the compact QED with dynamical fermions. In Monte Carlo (MC) calculations,²⁷ the order of the phase transition is of the first order on most of the critical line, and turns to second order like near its end point in the negative region of the adjoint representation. Also the noncompact QED seems to show a continuous transition.¹⁷ The MKRG also exhibits the qualitatively good phase structure. This approach, however, appears to be poor in its quantitative predictions. For example, away from the Wilson axis in the positive region of the adjoint representation, we found a stepwise transition in the β_1-t_G plot.^{13,22} It becomes continuous as one approaches the axis from above and becomes milder in the negative region. So the turning location from the sharp to milder transition seems to be shifted upward compared to the result of MC simulations, and thus the critical point on the Wilson axis looks second order, as shown in Fig. 8. We consider, therefore, that the results shown in this paper reflect the physics of the region closer to the second-order critical point obtained by MC simulations.

Our numerical computations become poor in precision at large number of RG steps because of the rapid movement of some parameters, particularly A . So the result of the RG flow in the figures shown in this paper are truncated within the reliable steps. We have therefore an analytic look at the recursion equations in the Appendix in order to make sure that there is an infrared stable fixed point in the strong four-Fermi coupling phase. In the intermediate region of the domain III, however, one cannot exclude a possibility that there might be other fixed points locating beyond our truncated region. This may be an interesting issue which is worth attacking by some other approaches such as the Monte Carlo renormalization-group method.

The renormalization-group approach provides the best understanding of the phase structure of field theory regularized on the lattice. It is therefore important to go beyond the qualitative step of the approximated RG approach such as MK in order to obtain more accurate knowledge. There is some way to improve MKRG (Ref. 28). Also some attempts based upon real-space or momentum-space RG approaches have been made in gauge-fermion systems,²⁹⁻³¹ although these are of a different context from the present paper.

ACKNOWLEDGMENTS

The authors are grateful to K. Ghoroku, K. Funakubo, and the theory group of Kyushu University for valu-

able discussions. H.Y. was partially supported by Grant-in-Aid for Encouragement of Young Scientists of the Ministry of Education, Science, and Culture (No. 01740161).

APPENDIX

The recursion equations (2.11) are rather intricate. By using normalized couplings M and G , however, they become quite simple. In this appendix we present analytic forms for the fermionic recursion equations, and show that there exist infrared stable fixed points in the strong ($G \rightarrow \infty$) four-Fermi coupling limit.

Let the four-Fermi coupling before each RG transformation be G and the mass parameter be M . Consider a transformation $(G, M) \rightarrow (G', M')$, which consists of decimations, convolution with the plaquettes, and bond moving. It is convenient to define normalized quantities $G^{(i)}$ and $M^{(i)}$ ($i = 1, \dots, 4$) at each stage of decimations in (2.11) by $G^{(i)} \equiv C^{(i)} / A^{(i)2}$ and $M^{(i)} \equiv B^{(i)} / A^{(i)}$. They are successively given by

$$\begin{aligned} G^{(1)} &= -(G+1)^2 + 1, \\ G^{(2)} &= (G+1)^3 - 1, \\ G^{(3)} &= -(G+1)^4 + 1, \\ G^{(4)} &= (G+1)^5 - 1, \end{aligned} \quad (\text{A1})$$

and

$$\begin{aligned} M^{(1)} &= 2M^2 + G + 1, \\ M^{(2)} &= M^{(1)}M + \frac{M^{(1)2} + G^{(1)} - 1}{2M}, \\ M^{(3)} &= 2M^{(2)}M + \frac{2M^{(2)}M(G+1) + (G^{(2)} + 1)}{M^{(1)} + 2M^2}, \\ M^{(4)} &= 2M^{(3)}M + \frac{M^{(3)}(M^{(1)} + 2M^2)(G+1) + (G^{(3)} - 1)}{4M^{(1)}M}. \end{aligned} \quad (\text{A2})$$

Convolutions with the gauge field (2.13) yield

$$G_G \equiv \frac{C_G}{A_G^2} = \frac{G^{(4)} - [1 - (\bar{F}_1 / \bar{F}_0)^{2\lambda}] \epsilon_+ \epsilon_-}{(\bar{F}_1 / \bar{F}_0)^{2\lambda}} \quad (\text{A3})$$

and

$$M_G \equiv \frac{B_G}{A_G} = \frac{M^{(4)}}{(\bar{F}_1 / \bar{F}_0)^\lambda}. \quad (\text{A4})$$

These are further multiplied by a constant factor α due to the bond-moving procedure, yielding

$$G' = \alpha G_G, \quad M' = \alpha M_G. \quad (\text{A5})$$

When the four-Fermi coupling is large as in the case of the RG flow in the domain I, $G^{(i)}$ in (A1) become much simpler

$$G^{(i)} \approx G^{i+1} \quad (i = 1-4). \quad (\text{A6})$$

In the deeply strong-gauge-coupling region in the domain I, we found that the renormalized trajectory is given by $G \propto M^2$. So by letting $G = cM^2$ in (A2) one has

$$\begin{aligned} M^{(1)} &\approx (2+c)M^2, \\ M^{(2)} &\approx (4+3c)M^3, \\ M^{(3)} &\approx (c^2+8c+8)M^4, \\ M^{(4)} &\approx (5c^2+20c+16)M^5. \end{aligned} \quad (\text{A7})$$

Although both the G and M are affected by the vacuum polarization (A3) and (A4) its contribution cancels in the ratio G/M^2 :

$$\frac{G_G}{M_G^2} = \frac{G^{(4)}}{M^{(4)2}}. \quad (\text{A8})$$

Thus in the domain I the renormalized trajectory is given by

$$\frac{G'}{M'^2} = \frac{G^5}{\bar{c}M^{10}} = c', \quad (\text{A9})$$

where $\bar{c} = \alpha(5c^2 + 20c + 16)^2$ and $c' = c^5 / \bar{c}$. Therefore one finds that the RG transformation keeps the relation $G \propto M^2$, but that its proportional constant changes. This means that an infrared fixed point exists at $(G, M) = (\infty, \infty)$.

¹V. A. Miransky, *Nuovo Cimento* **A90**, 149 (1985).

²B. Holdom, *Phys. Rev. D* **24**, 1441 (1981).

³K. Yamawaki, M. Bando, and K. Matumoto, *Phys. Rev. Lett.* **56**, 1335 (1986).

⁴T. Akiba and T. Yanagida, *Phys. Lett.* **169B**, 432 (1986).

⁵W. A. Bardeen, C. N. Leung, and S. T. Love, *Phys. Rev. Lett.* **56**, 1230 (1986).

⁶C. N. Leung, S. T. Love, and W. A. Bardeen, *Nucl. Phys.* **B273**, 649 (1986).

⁷W. A. Bardeen, C. N. Leung, and S. T. Love, *Nucl. Phys.* **B323**, 493 (1989).

⁸K. G. Wilson and J. Kogut, *Phys. Rep.* **12C**, 75 (1974).

⁹A. A. Migdal, *Zh. Eksp. Teor. Fiz.* **69**, 810 (1975) [*Sov. Phys.*

JETP **42**, 413, (1976)]; **69**, 1457 (1975) [**42**, 743 (1976)].

¹⁰L. P. Kadanoff, *Ann. Phys. (N.Y.)* **100**, 359 (1976).

¹¹S. Caracciolo and P. Menotti, *Ann. Phys. (N.Y.)* **122**, 74 (1979).

¹²T. Matsui, *Nucl. Phys.* **B136**, 277 (1978).

¹³M. Imachi, S. Kawabe, and H. Yoneyama, *Prog. Theor. Phys.* **69**, 221 (1983); **69**, 1005 (1983).

¹⁴M. Imachi and H. Yoneyama, *Prog. Theor. Phys.* **78**, 623 (1987).

¹⁵K. M. Bitar, S. Gottlieb, and C. K. Zachos, *Phys. Rev. D* **26**, 2853 (1982).

¹⁶K. M. Bitar, S. Gottlieb, and C. K. Zachos, *Phys. Lett.* **121B**, 163 (1983).

- ¹⁷J. B. Kogut, E. Dagotto, and A. Kocić, Nucl. Phys. **B317**, 253 (1989).
- ¹⁸J. B. Kogut, E. Dagotto, and A. Kocić, Nucl. Phys. **B317**, 271 (1989).
- ¹⁹S. P. Booth, R. D. Kenway, and B. J. Pendleton, Phys. Lett. B **228**, 115 (1989).
- ²⁰A. M. Horowitz, Phys. Lett. B **219**, 329 (1989).
- ²¹S. Hands, J. B. Kogut, and E. Dagotto, Nucl. Phys. **B333**, 551 (1990).
- ²²M. Imachi, Prog. Theor. Phys. **81**, 1225 (1989).
- ²³J. Kogut and L. Susskind, Phys. Rev. D **11**, 395 (1975).
- ²⁴L. Susskind, Phys. Rev. D **16**, 3031 (1977).
- ²⁵K-I. Kondo, H. Mino, and K. Yamawaki, Phys. Rev. D **39**, 2430 (1989).
- ²⁶Y. Nambu and G. Jona-Lasinio, Phys. Rev. **122**, 345 (1961).
- ²⁷M. Okawa, Phys. Rev. Lett. **62**, 1224 (1989).
- ²⁸G. Martinelli and G. Parisi, Nucl. Phys. **B180**, 201 (1981).
- ²⁹K. Kanaya (unpublished).
- ³⁰K-I. Aoki, Report No. RIFP-758, 1988 (unpublished).
- ³¹Y. Sugiyama, Phys. Lett. B **223**, 445 (1989).